Available online at www.sciencedirect.com

ScienceDirect

Energy Procedia 135 (2017) 92–104

Energy Procedia

www.elsevier.com/locate/procedia

11th International Renewable Energy Storage Conference, IRES 2017, 14-16 March 2017, Düsseldorf, Germany

Unlocking flexibility by exploiting the thermal capacity of concrete core activation

B. van der Heijde[a,b,c,*], M. Sourbron[a,b], F.J. Vega Arance[b,*], R. Salenbien[a,c], L. Helsen[a,b]

[a] *EnergyVille, Thor Park, Poort Genk 8310, 3600 Genk*
[b] *Mechanical Engineering Department, KU Leuven, Celestijnenlaan 300 box 2421, 3001 Leuven*
[c] *VITO NV, Boeretang 200, 2400 Mol*

Abstract

Due to its inherent large thermal inertia, concrete core activation (CCA) could assist in active demand response schemes. By shifting the injection or extraction of thermal power in time, demand peaks that normally occur more or less simultaneously in clusters of buildings can be spread out in time. Furthermore, thanks to the low temperature differences allowed with respect to the room temperature, CCA is ideally combined with technologies that have increasing renewable potential, such as heat pumps, low temperature district heating and high temperature district cooling. This paper illustrates the flexibility potential of concrete core activation through the exploitation of its thermal energy storage capacity by dynamic simulations. A validated RC thermal model of a CCA is coupled with a detailed building model, including user occupancy and weather disturbances. The flexibility indicator is calculated based on a method presented in the literature, but using an extended version that allows application to more complex systems, including heat losses. Balancing the building between minimal and maximal temperature, the thermal power needed to heat or cool the building can be modulated up- or downward with respect to the reference energy use. The method is applied to various building types with different insulation levels, in order to map the flexibility potential of CCA heating compared to buildings heated with radiators.

Peer-review under the responsibility of EUROSOLAR - The European Association for Renewable Energy.

Keywords: Flexibility, Thermally Activated Building Systems (TABS), Concrete Core Activation (CCA), Optimal control, Active Demand Response (ADR)

1. Introduction

The energy system is currently in a transition towards the use of more renewable energy sources. The variability and unpredictability of these sources pose challenges to the security of supply and to balancing demand and supply of the energy grid. As part of the solution, flexibility can be introduced, using energy storage or active demand response. One technology that combines both is the activation of the thermal inertia of buildings as heat or cold storage, as studied by e.g. Reynders *et al.* [1] and Patteeuw *et al.* [2,3]. Ahcin and Sikic [4] show how demand response can be

* Corresponding author. Tel.: +32-16-373230
E-mail address: bram.vanderheijde@energyville.be

1876-6102
Peer-review under the responsibility of EUROSOLAR - The European Association for Renewable Energy.
10.1016/j.egypro.2017.09.490

incorporated in the context of the *Energy Hub* [5] model. An interesting take on the load shifting potential based on the minimal and maximal daily load curve of a domestic hot water boiler has been studied by D'Hulst *et al.* [6].

Stinner *et al.* [7] present a comprehensive literature study on flexibility indicators in the built environment, showing that the concept is not unambiguously defined. De Coninck and Helsen [8] the increase in cost with respect to the cost-optimal heating and cooling profile to quantify flexibility and its economic value in houses with heat storage buffers. Nuytten *et al.* [9] calculate the flexibility of a district supplied by a CHP (Combined Heat and Power system) and incorporating central or localized heat storage tanks by means of the maximal time during which consumption can be increased to the nominal power of the supply unit or decreased to zero based on the predetermined heat load curve. The buffer tanks are assumed to be perfectly mixed and insulated, hence heat losses are neglected, which greatly simplifies the calculation of these flexibility curves to interpolating between two piecewise linear load curves. Stinner *et al.* [7] further elaborate this method and apply it to a building with a heat storage tank, looking at flexibility from a temporal, power and energy perspective, always with respect to a reference energy use profile from a dynamic simulation in Modelica. Because of multiple possible objectives, such a reference profile is not straightforwardly defined for the building studied in this paper. Indeed, when the objective is to minimize energy, a different heat load would be found than for a minimal cost objective in a scenario with varying energy prices.

Thermally activated building systems (TABS) are considered particularly beneficial in the context of providing flexibility [10–12]. These papers studied the example of CCA, in which concrete floors are equipped with pipes through which warm or cold water is pumped in order to heat or cool the adjacent rooms. An advantage of this system is that small temperature differences with respect to the room temperature are sufficient for heating and cooling, which opens perspectives for highly efficient, low temperature heat and high temperature cold supply systems, e.g. heat pumps or fourth generation thermal networks.

The flexibility is provided by the increased building thermal mass in heavy concrete floors, but the drawback thereof is the large time constant which hampers the control of the emission system. In addition, only the thermal input is controlled, while the amount and time of heat emission cannot be decided. These drawbacks are handled by advanced control algorithms such as Model Predictive Control (MPC), as studied by for example Sourbron [13] and Sturzenegger *et al.* [14]. Controller models for TABS, and CCA in particular, have been proposed and validated by Koschenz and Lehmann [15], Weber and Jóhannesson [16,17] and Sourbron *et al.* [18]. Work regarding CCA as a storage system providing flexibility has been carried out earlier by van der Heijde *et al.* [19] and Vega [20], by means of defining and quantifying a State-of-Charge (SoC) for this system.

The current paper aims at investigating the maximal flexibility provided by a CCA floor in a residential building for the case of heating only, regardless of the heat production system and of the price of energy, compared to a conventionally heated building. Therefore, the method from Nuytten *et al.* [9] and Stinner *et al.* [7] is adopted and extended. This extension is needed because the complexity of the building structure implies multiple time constants and the heat losses can in this case not be neglected. Therefore, the linear equations are extended to a dynamic calculation.

Nomenclature

CHP	Combined Heat and Power
CCA	Concrete Core Activation
MPC	Model Predictive Control
NZEB	Nearly Zero Energy Building
RC	Resistance-Capacitance
SoC	State of Charge
SD	Semi-Detached building typology
TABS	Thermally Activated Building System

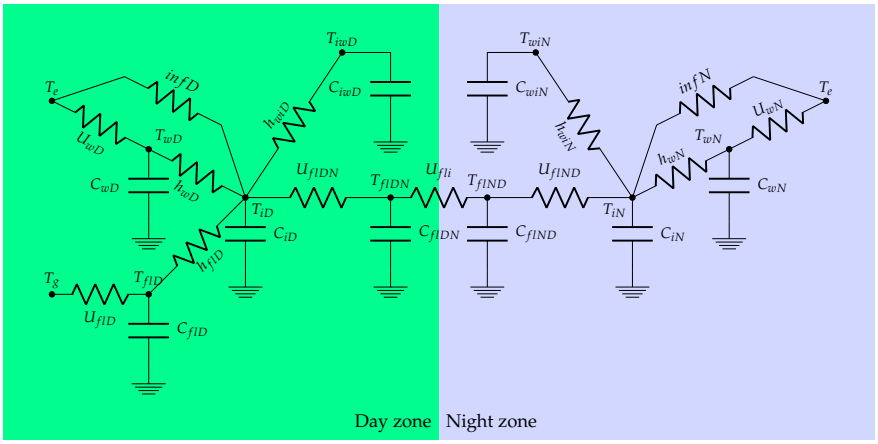

Fig. 1. Schematic representation of the original model [21], excluding the added floor nodes for TABS.

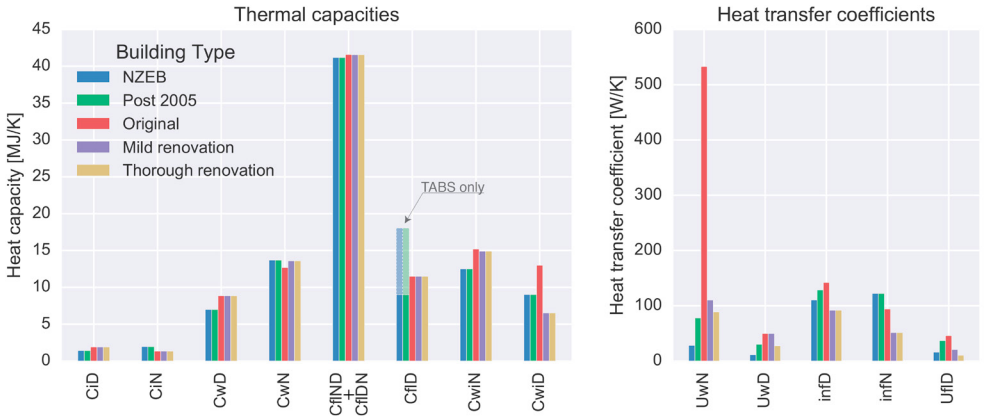

Fig. 2. Comparison of key thermal capacities and heat transfer coefficients for the studied buildings.

2. Methodology

2.1. Building model

The building models employed for this study are based on the resistance-capacitance representations by Reynders *et al.* [21,22], considering the TABULA typical Belgian residential building typologies [23] (see Fig. 1). Different semi-detached building types are compared. For the older buildings (SD4 from Protopapadaki *et al.* [24]) and the mild and thorough renovation thereof, conventional heating with radiators is assumed. For the more recent buildings – SD5, built after 2005, and SD6, Nearly Zero Energy Building (NZEB) –, TABS and radiators are compared.

Since the emphasis lies on the additional flexibility provided by the concrete floor activation, this part is modelled in more detail. The floor nodes of the original model redistributed into three thermal capacities for each floor, respecting the original heat transfer coefficient by Reynders [25]. A selection of the parameter values for the 5 studied building topologies is summarized for comparison in Fig. 2.

The thermal mass of the day (occupation) zone floor, originally only about 1/4 to 1/3 of that of the floor between day and night zone, is doubled in order to have a more representative thermal capacity for this TABS element. Notice the remarkably high heat transfer coefficient U_{wN} in the "Original" building type, which is caused by the uninsulated roof.

Table 1. Occupant heat gains and comfort boundaries on room temperature, assuming 4 occupants. Light grey indicates occupancy, dark grey absence.

Hour	Day zone		Night zone	
	Temperature [°C]	Heat gains [W]	Temperature [°C]	Heat gains [W]
0 – 7	16 – 24	200	18 – 20	360
7 – 9	21 – 23	835	16 – 24	135
9 – 17	16 – 24	200		
17 – 22	21 – 23	835		
22 – 0	16 – 24	200	18 – 20	360

2.2. Boundary conditions and constraints

A typical meteorological year from the weather station of Uccle, Belgium provides the ambient temperature T_e and solar radiation data. The ground temperature T_g is assumed constant at 12 °C. The direct and diffuse solar radiation are projected onto the four exterior wall surfaces and these solar gains are distributed over the model capacities as described by Reynders *et al.* [1,21]. Heat gains from occupants and zone temperature constraints are determined from a hypothetical inhabitant presence and varied according to a fixed time schedule, see Tab. 1. For further details on the distribution of solar and occupant heat gains over the model nodes, as well as the heat from the radiators, the reader is referred to the respective original publications ([1,21]).

Comfort temperature ranges are derived from Reynders *et al.* [21] and Patteeuw [26]. A distinction is made between *narrow bounds*, which refers to the constraints in Tab. 1, and *wide bounds*, in which 16-24 °C is widened to 14-28 °C during absence. The heat gains are adapted from Deurinck [27] and kept constant during the respective time slots and across all building types; for a more representative analysis, heat gain profiles could be constructed according to Baetens and Saelens [28], but this was omitted for simplicity. Nevertheless, the used implementation allows easy adaptation of these constraints. This allows e.g. increasing the comfort temperatures during the warm season.

For a building with radiator heating, the maximal power is calculated from the design case, i.e. the steady state heat demand for an indoor temperature of 20 °C and 18 °C for day and night zone and a worst-case outdoor temperature of −10 °C, based on the Belgian climate. For CCA, a maximal heating power of 35 W m^{-2} is assumed, based on Franck [29], from which the nominal heating power is derived by multiplying with the total building heated floor area.

2.3. Flexibility

In this paper, flexibility is defined as the ability of a thermal system to use more or less energy than in a given reference energy use profile. The former is referred to as upward flexibility, the latter as downward. This paper approaches energy from the end user side: it only considers heating energy, without looking at the primary energy needed to get the energy into the building. However, defining a reference energy use profile is not so obvious as in the case studied by Nuytten *et al.* [9], where the tank is either empty or full at the start of an iteration, and the heat demand is known in advance. Here, multiple capacities in the building model and varying heat losses to the surroundings result in a higher complexity. This also entails that the net amount of energy used when the system is tracking the maximum temperature is considerably larger than that of the minimal temperature case. As explained by Patteeuw [2], the actual minimum and maximum temperature band become narrower because of the slow system dynamics (see later in Fig. 4): since the thermal power delivered to or lost from the building is limited, the temperatures cannot change immediately and the controller needs to anticipate changes. In the case of a very high building mass, as is the case with TABS, this translates into the observation that the widened temperature range during absence is barely used. In the following subsections, first the calculation of several possible upward and downward flexibility indicators is explained. Thereafter, the estimation of the maximal flexibility potential is elaborated.

2.3.1. Calculation of flexibility

As described by Stinner *et al.* [7], there are different ways to express flexibility, namely:

1. time during which the thermal input is minimal or maximal,
2. average power shifted with respect to reference use profile and
3. difference in energy use with respect to the reference use profile.

It is assumed that the building already has a reference energy use profile – the thermal power input profile minimizing e.g. cost or energy use – and that the activation of flexibility makes the actual energy use profile diverge from the reference profile. The reference state trajectory refers to the state trajectory corresponding to the heat input from the reference energy use profile. Upward flexibility refers to increased energy use with respect to the reference, downward to decreased energy use. Section 2.3.2 clarifies the reference profiles used to assess the maximal flexibility potential.

The upward temporal flexibility indicator t_{flex}^{up} is defined as the time period during which the heating can be switched on at maximal power. It is calculated from maximizing the zone temperatures starting from the reference state trajectory (initialization $\boldsymbol{x}_0$) at the beginning of the flexibility activation and logging the time during which the thermal output is maximal:

$$
\begin{aligned}
\max_{\boldsymbol{x},\boldsymbol{u}} \quad & \sum_t \left(T_{iD,t} + T_{iN,t} - M \sum_j \varepsilon_{j,t} \right) \\
\text{subject to} \quad & \boldsymbol{x}_t = A\boldsymbol{x}_{t-1} + B \begin{bmatrix} \boldsymbol{u} \\ \boldsymbol{d} \end{bmatrix}_{t-1}, \quad \forall\, t > 0 \\
& \boldsymbol{x}_0 = \text{Initial conditions from reference state trajectory} \\
& \underline{T}_{iN,t} - \underline{\varepsilon}_{iN,t} \leq T_{iN,t} \leq \overline{T}_{iN,t} + \bar{\varepsilon}_{iN,t}, \quad \forall\, t \\
& \underline{T}_{iD,t} - \underline{\varepsilon}_{iD,t} \leq T_{iD,t} \leq \overline{T}_{iD,t} + \bar{\varepsilon}_{iD,t}, \quad \forall\, t \\
& \varepsilon_{j,t} \geq 0, \quad \forall\, j,t \\
& \sum_j u_{j,t} \leq \bar{u},
\end{aligned}
\tag{1}
$$

in which the following symbols are used: $T_{iD,t}$ and $T_{iN,t}$ are the day and night zone temperature, both of which are represented in the state vector $\boldsymbol{x}_t$ alongside all other temperature states. The temperature parameters with a bar underneath or above refer to the lower and upper comfort boundaries at time t, as defined in Tab. 1. M is an arbitrarily large number to penalize the slack variables $\varepsilon_{j,t}$ sufficiently with respect to the real objective. These slack variables are needed to find a solution at all times, thereby occasionally allowing overheating or undercooling. The subscript j refers to the different slack variables on the minimal and maximal temperature of day and night zone respectively. A and B are the state-space representation matrices with respect to the states $\boldsymbol{x}_t$, the control actions $\boldsymbol{u}_t$ (i.e. the heat flow to the core of the lower and upper CCA) and disturbances $\boldsymbol{d}_t$ (ground and ambient temperature, occupant and solar heat gains). These matrices are the discrete time representation of the RC model with a time step of 15 minutes. Finally, the sum of the control actions $\boldsymbol{u}_t$ is limited to the maximal power of the heating system $\bar{u}$ as defined in Section 2.2. The optimization problem is limited to a pre-set time horizon. In addition to the constraints listed above, the CCA floor temperatures are constrained to 29 °C at the surface and 45 °C at the core [29]. The constraint on the core temperature aims to limit the temperature of the supply water to the CCA, so as to enable the use of a high efficiency heat production system, while the surface temperature is a comfort consideration.

Fig. 3 illustrates the definition of t_{flex}^{up} and t_{flex}^{down} (see below), starting from an arbitrary initial state. The time instants of t_{flex} are shown where the temperature trajectory is about to cross one of the comfort boundaries. t_{flex} can also be reached when there is no comfort boundary violation yet, but when the optimization problem foresees a future violation if the heat output stays at the current level. In both cases, the power output level of the heating system needs to be changed in order to comply with the comfort constraints.

For the downward temporal flexibility indicator t_{flex}^{down}, the zone temperatures are minimized starting from the reference state trajectory and the time period during which the thermal output is zero is logged. The temperature mini-

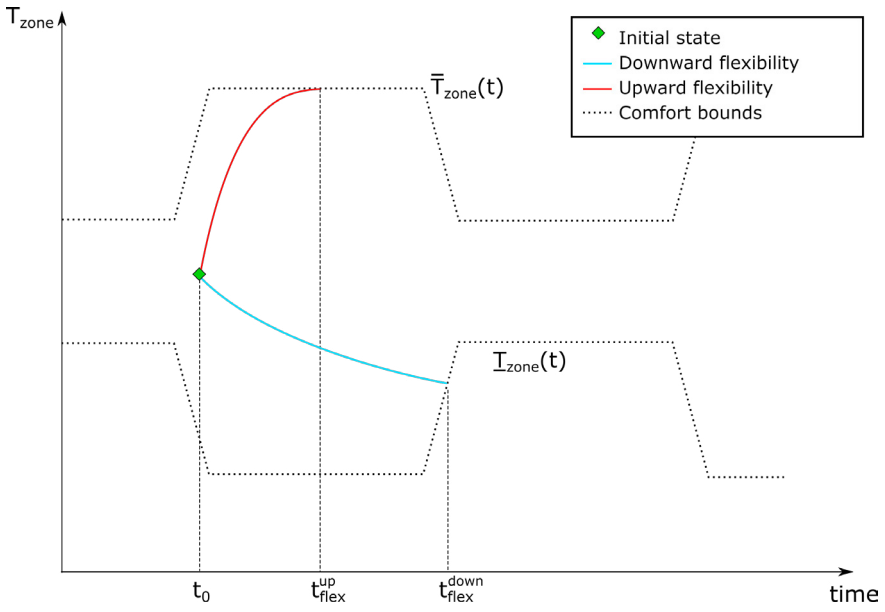

Fig. 3. Illustration of the calculation of t^{up}_{flex} (max. heating power) and t^{down}_{flex} (heating system off) starting from an arbitrary initial state.

mization is given as:

$$\min_{\boldsymbol{x},\boldsymbol{u}} \sum_{t} \left(T_{iD,t} + T_{iN,t} + M \sum_{j} \varepsilon_{j,t} \right), \tag{2}$$

for which the constraints are the same as those in Eq. (1). As soon as any of the constraints is reached in (1) or (2), the heating system has to adjust its output, which will no longer be maximal or minimal respectively.

A fair comparison of flexibility in different buildings requires that the nominal heating power is taken into account, since a building with a higher nominal power provides more flexibility in terms of energy than one with a lower power for the same upward temporal flexibility. The downward flexibility is more complicated, since it is linked to how fast the building cools down, which depends on its thermal mass, insulation and ambient temperature. The energy difference between the reference and the respective upward and downward flexibility action amounts to the integrated difference of their power use profiles:

$$\Delta E^{down}_{flex}(t, t_0) = \int_{t_0}^{t} \left(P_{ref}(\vartheta) - P_{min}(\vartheta) \right) d\vartheta \quad \text{or} \tag{3}$$

$$\Delta E^{up}_{flex}(t, t_0) = \int_{t_0}^{t} \left(P_{max}(\vartheta) - P_{ref}(\vartheta) \right) d\vartheta, \tag{4}$$

where ϑ is the integration variable, t_0 and t the initial and variable time, and $P_{max}(t)$ and $P_{min}(t)$ the maximal and minimal heating power injection resulting from the optimization at time t. $P_{ref}(t)$ represents the reference power profile.

The definition is chosen such that ΔE_{flex} is non-negative regardless of the direction of the flexibility action. The three indicators are adapted from Stinner *et al.* [7]. It can easily be verified that ΔE_{flex} does not decrease as long as $t \leq t_{flex}$. This energy is partly stored in or discharged from the thermal capacity of the building, and partly lost to the environment. Evidently, the energy losses are higher for a higher average temperature of the building components, and thus for the maximal flexibility trajectory. Therefore, ΔE_{flex} must not be interpreted solely as the energy stored in the building mass. Notice that ΔE_{flex} must not always increase, but it must always be larger than or equal to 0 because of its definition.

ΔE_{flex} can be used to calculate the average flexible power available at some point in time as a third flexibility indicator:

$$\left\langle P_{flex}^{\{up,down\}} \right\rangle (t, t_0) = \frac{\Delta E_{flex}^{\{up,down\}}(t, t_0)}{t - t_0}, \tag{5}$$

in which the bracket notation denotes the time average. $\left\langle P_{flex} \right\rangle$ reaches a maximum when $t - t_0 \leq t_{flex}$. From then on the average power will start declining and approaches the difference in heat losses between the flexibility trajectory and the reference. $\left\langle P_{flex} \right\rangle_{max}$ is limited by the maximal heat input.

Additionally, Stinner *et al.* [7] define a cycle flexibility, in which an upward or downward flexibility action is followed by another one in the opposite direction. This allows to better interpret the importance of heat losses due to flexibility activation. Indeed, following a flexibility activation, the reference power profile and state trajectory should be recalculated using the final state after the activation. This is however not treated further in this paper, as explained in the next section.

2.3.2. Estimation of maximal flexibility potential

The maximal flexibility potential is estimated by means of the maximal upward and downward temporal flexibility starting from every hour of the studied period, making abstraction of energy price or CO_2 emissions. Therefore, two reference power profiles and corresponding state trajectories are needed: the maximal temperature trajectory from which t_{flex}^{down} is calculated, and the minimal temperature for t_{flex}^{up}. This can be compared to the approach of Nuytten *et al.* [9], where the storage tank is either full or empty at the start of every flexibility activation in order to assess the maximal potential. In addition, the energy difference and average flexible power are calculated for every hour, using the temporal flexibilities as respective integration intervals: $\Delta E_{flex}^{\{up,down\}}\left(t_0 + t_{flex}^{\{up,down\}}, t_0\right)$ and $\left\langle P_{flex}^{\{up,down\}} \right\rangle \left(t_0 + t_{flex}^{\{up,down\}}, t_0\right)$ where t_0 denotes the time step at which the flexibility calculation is started.

While reinitialization for every time step is not realistic, it allows making a fair comparison between different building types. The indicators mentioned above are calculated for every hour with the optimization for quarter-hourly time steps, with a control horizon of 48 h. The value of this horizon is chosen so as not to cut off the temporal flexibility to the value of the horizon. In addition, the temperature constraints on the day and night zone temperature are replaced by the corresponding maximum and minimum temperatures from the reference state trajectory. Otherwise, a sudden fall or rise in the constraints outside the optimization horizon might not be foreseen, leading to a higher perceived flexibility.

3. Results

In this section, first the reference calculations and the resulting solutions of the maximal and minimal flexibility are illustrated for clarity. Afterwards, the results found for different buildings, months and boundary conditions are summarized and compared.

3.1. Example

Fig. 4 shows an example of the steps described above. The 15th of February at 6 PM has been chosen as the starting point for the flexibility activation, and the dash-dotted lines indicate the comfort constraints in both zones for the 48 h horizon. In the two upper diagrams, the upper solid line shows the maximum reference for the zone temperatures, the lower solid line the minimal. The marked lines show the trajectories of the flexibility calculations: the downward flexibility activation, marked with squares, starts at the maximal temperature and then free-floats to the lower bound. A similar pattern is followed for the upward flexibility action, marked with circles, but in the opposite direction.

The two lower graphs show how much energy is injected into the building in addition to the minimal reference energy use profile or short of the maximal reference and the respective average power flexibility. The upward temporal flexibility is 14 h, downward 16.5 h. After these intervals, the respective cumulative energy difference decreases for the first time during the time horizon. Fig. 4 shows that depending on which value should be maximized – time duration at max/min power, energy difference or average power – different results for the optimal flexibility duration

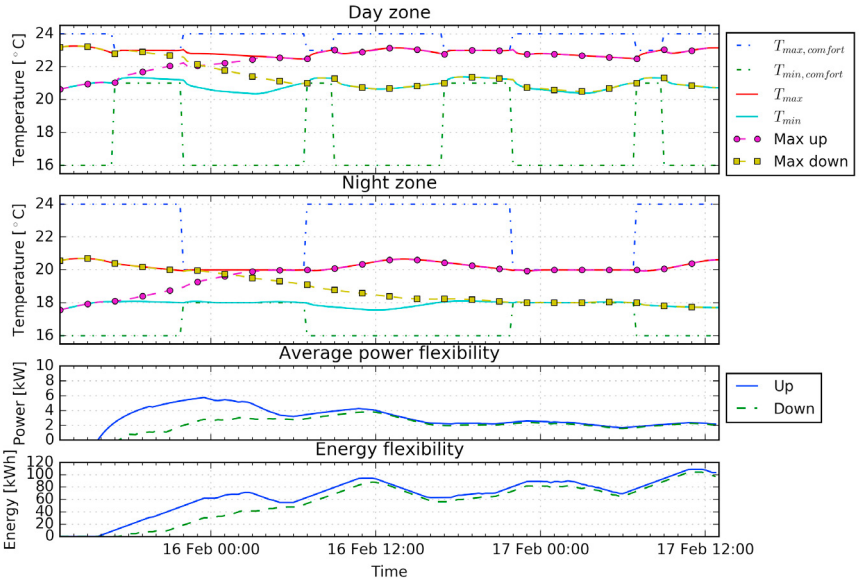

Fig. 4. Illustration of maximal and minimal temperature sequencemaximal and minimal reference state trajectories for day and night zone temperature, as well as the corresponding upward and downward flexibility sequences. The lower graphs show ΔE_{flex} and $\langle P_{flex} \rangle$ for the two cases.

are found. Notice that the average power and energy flexibility remain zero during the first hours, during which the heat input in the flexibility action is the same as that of the reference.

3.2. Parameter study

This section presents the results regarding the three flexibility indicators and how they are influenced by building construction and heating parameters, month and spread of the temperature bounds. Three winter months were chosen because flexibility in summer months is very low for a heating case. The distribution is presented in violin plots, which do not only show the approximate distribution of the values, but also the quartile and median values (shown by the dashed horizontal lines). The left and right side of each "violin" correspond to the flexibility as calculated from the minimal or maximal reference. Finally, the plots for buildings with radiators are blue, those with TABS are green.

Fig. 5 shows the distribution of the temporal flexibility: t^{up}_{flex} from the minimal reference and t^{down}_{flex} from the maximal reference. In general, the upward flexibility is spread out more than the downward flexibility. While the distribution of t^{up}_{flex} decreases with the month, t^{down}_{flex} goes up. The influence of wide or narrow bounds (lower and upper row) is low for the buildings with TABS as seen in the 4$^{\text{th}}$ and 6$^{\text{th}}$ column of Fig. 5, but the influence on buildings heated with radiators is visible. The on-time seems to be pushed towards slightly lower values, while the off-time increases overall for wider comfort bounds. Comparing the post 2005 and NZEB buildings with TABS and radiators, it appears that more upward and downward flexibility is provided by TABS.

Flexibility can also be compared by the energy use which is shifted forward or backward in time during the flexibility operation, see Equations (3) and (4). Indeed, different building types have a different nominal power, therefore the temporal flexibility corresponds to a different energy flexibility. The energy differences between the flexibility action and the reference (again for the maximal and minimal reference) are shown in Fig. 6.

These results clearly show a decreasing spread and average flexibility with increasing insulation for buildings with radiators; the buildings with TABS have a much more concentrated flexibility. The monthly variation is less outspoken for the downward than for the upward flexibility. The moderate variation of the temporal flexibility with the change in comfort bounds is translated to a more substantial change here, at least for buildings with radiators. The newer buildings with TABS have slightly higher downward energy flexibility than their counterparts with radiators. On the other hand, the upward flexibility is higher on average for the radiator-heated buildings. The reason for this is not

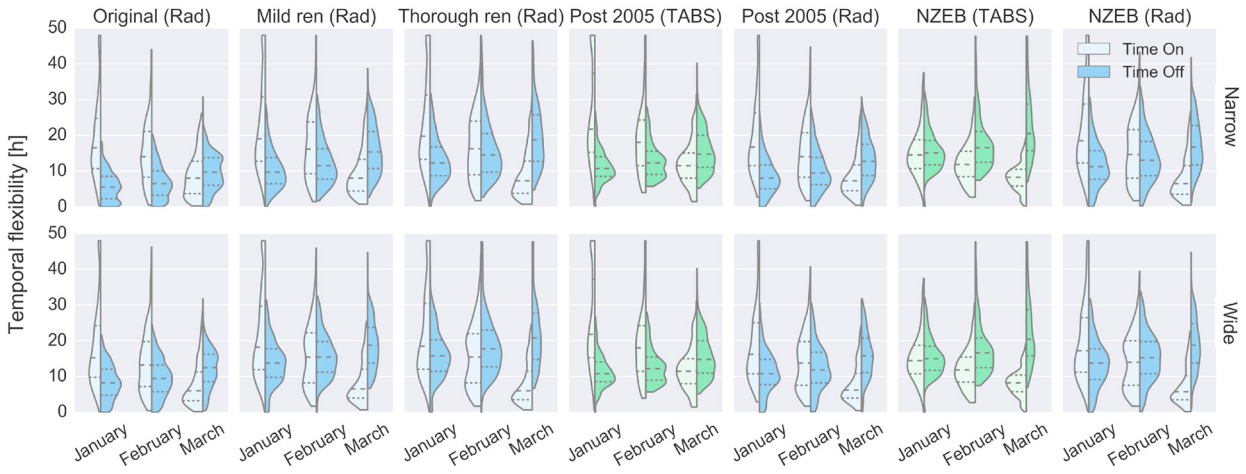

Fig. 5. Distribution of maximal on/off time for different buildings, months and temperature constraint variations.

Fig. 6. Distribution of energy flexibility during maximal on/off time.

immediately clear, but it is expected that because radiators heat up different external building parts more easily due to the radiative and convective distribution, the buildings with radiators also experience more heat losses.

The distribution of $\langle P_{flex} \rangle$ is shown in Fig. 7, where the nominal power for the different building types can clearly be seen as the upper limit. Here, an opposite trend for subsequent months with respect to temporal and energy flexibility can be seen, namely an increase in average power flexibility for the minimal reference, and a decline for the maximal reference. The NZEB has comparable maximal power output for the radiator and TABS implementation, but still the average power flexibility is higher for the buildings with radiators, certainly regarding upward flexibility.

The violin plots are an interesting tool to identify general trends, however the time correlation of the results is lost. Heat maps can be used to display the time evolution of the variables presented above. They allow easy comparison for the same hour or for the same day. Fig. 8 allows to identifyidentifying similar hourly and daily patterns in maximal upward flexibility, supposedly varying similarly with ambient temperature and solar gains. The darkest red corresponds to the highest value encountered in all violin plots, applying the same colour scale to all graphs. t^{up}_{flex} is the highest on average for the post 2005 building with TABS. The renovated older buildings also score high on this indicator, and even higher than the newest buildings with radiators as a matter of fact. For downward flexibility, the TABS buildings seem the most interesting option because of their relatively high thermal mass, again with the renovated older buildings as runner-up. For t^{down}_{flex} (Max Ref), the buildings with radiators still display clear patterns

Fig. 7. Distribution of average power flexibility during maximal on/off time.

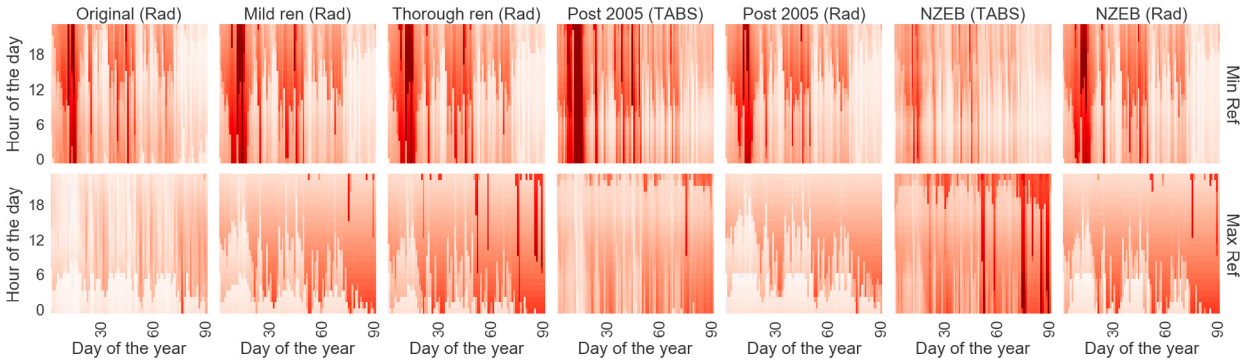

Fig. 8. Evolution of maximal heat supply delay or advance in time.

around 7 AM, where the comfort constraints change. Buildings with TABS behave much more smoothly, reflecting the limited spread observed in Fig. 6.

The darkest red[1] corresponds to the highest value encountered in all violin plots, applying the same colour scale to all graphs. t^{up}_{flex} is the highest on average for the post 2005 building with TABS. The renovated older buildings also score high on this indicator, and even higher than the newest buildings with radiators as a matter of fact. For downward flexibility, the TABS buildings seem the most interesting option because of their relatively high thermal mass, again with the renovated older buildings as runner-up. For t^{down}_{flex} (Max Ref), the buildings with radiators still display clear patterns around 7 AM, where the comfort constraints change. Buildings with TABS behave much more smoothly, reflecting the limited spread observed in Fig. 6.

4. Discussion

Firstly, the flexibility has only been calculated for a selection of winter months. During summer, all buildings demonstrate overheating due to the unchanged comfort settings. Since the maximal and minimal reference coincide during overheating, there is no heating flexibility in that case. The introduction of higher comfort temperature limits and cooling is needed to allow flexibility to be used in the warmer season.

[1] The colour scale was omitted deliberately since the information in these graphs is rather in the patterns and relative changes than in the absolute values they represent.

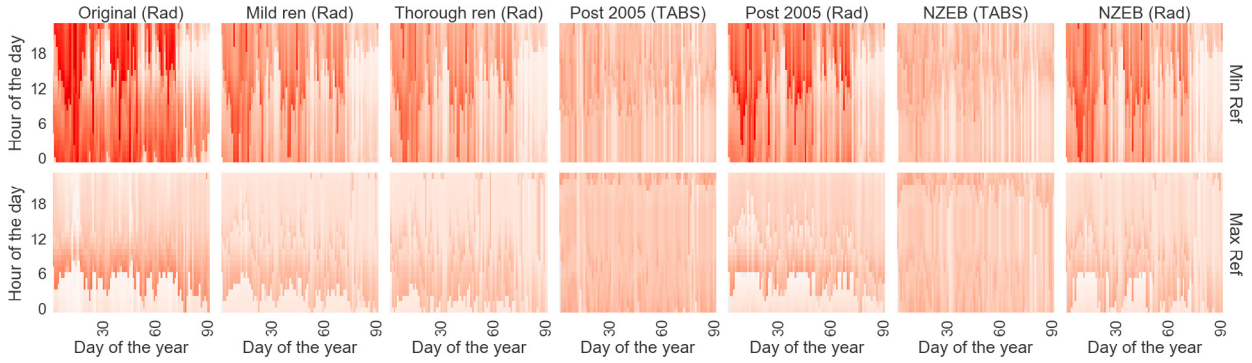

Fig. 9. Evolution of postponed or sped-up energy supply.

Furthermore, although it seems that older buildings with radiators provide more flexibility, it must be noted that this is largely the result of higher energy losses in less insulated buildings. This results in a trade-off between flexibility and energy efficiency. Further study towards the role of heat losses in these calculations, e.g. for consecutive charging/discharging cycles, would allow a more thorough comparison. The influence of the widened bounds during absence is limited in radiator-heated buildings, and absent in those with TABS. It is expected that the comfort settings during occupancy have more influence, but these settings are unlikely to be changed in order to access flexibility.

The variation in results for different flexibility indicators reflects different potential uses of these values. For instance, a grid operator who wants to up- or downscale the immediate energy use because of a sudden change in the availability of renewable energy sources wont worry about the energy difference during this flexibility activation; he seeks how many customers are able to consume at maximal or minimal power and for how long. Another operator who is rather interested in peak shaving will be looking at energy differences with respect to the planned or predicted energy use pattern. Before the step towards the grid is made, these calculations in terms of heat delivery must first be translated to variables at the grid side. For thermal networks, this includes losses at the generation side, during transport and in heat exchangers. For electricity, heat pumps and CHP units should be modelled and their electric in- or output assessed as in Stinner *et al.* [7].

Finally, the insights provided by the dynamic calculations for different building types lead the authors to relativize the usefulness of an SoC indicator as defined previously by van der Heijde *et al.* [19] for TABS. Whereas Vega [20] extended this definition based on steady-state behaviour, it is found that this steady-state is rarely reached during normal building use. Instead, it would be more correct to assess the potential for storing or discharging heat in the building by means of ΔE_{flex}, which allows making a relevant calculation from any arbitrary initial state and for any desired time interval.

5. Conclusion and further recommendations

In conclusion, this paper presents the extension of existing frameworks for quantifying flexibility of thermal systems, applied to activated residential building mass in particular. The scientific contribution exists in the application to more complex models including detailed dynamic behaviour and heat losses, without limiting the range of applications to buildings. Different building types and temperature constraint settings have been compared and it follows that although less insulated buildings heated with radiators show a higher flexibility potential overall, buildings heated with TABS are more flexible when compared to the same construction type with radiators.

Further recommendations include expanding the study to variable comfort limits for winter and summer and including a cooling system. As described in the Discussion section, the grid side can be accounted for as well with some extra assumptions and variable price profiles can be included to further study the value or cost of flexibility. Finally, the cycle efficiency from Stinner *et al.* should be adapted in this study as well.

Acknowledgements

The authors gratefully acknowledge the financial support for the work of Bram van der Heijde by the European Union, the European Regional Development Fund ERDF, Flanders Innovation & Entrepreneurship and the Province of Limburg through the project 'Towards a Sustainable Energy Supply in Cities'. Furthermore, VITO is gratefully acknowledged for the financial support of Bram van der Heijde through a PhD Fellowship. Finally, the authors would like to thank Glenn Reynders and Dieter Patteeuw for their highly appreciated input.

References

[1] Reynders, G., Nuytten, T., Saelens, D.. Potential of structural thermal mass for demand-side management in dwellings. Building and Environment 2013;64:187–199. URL: http://dx.doi.org/10.1016/j.buildenv.2013.03.010. doi:10.1016/j.buildenv.2013.03.010.

[2] Patteeuw, D., Helsen, L.. Residential buildings with heat pumps, a verified bottom-up model for demand side management studies. In: 9th International Conference on System Simulation in Buildings (SSB), Liège. Liège (Belgium); 2014, p. 1–19. URL: https://lirias.kuleuven.be/handle/123456789/473921.

[3] Patteeuw, D., Bruninx, K., Arteconi, A., Delarue, E., D'haeseleer, W., Helsen, L.. Integrated modeling of active demand response with electric heating systems coupled to thermal energy storage systems. Applied Energy 2015;151:306–319. URL: http://dx.doi.org/10.1016/j.apenergy.2015.04.014. doi:10.1016/j.apenergy.2015.04.014.

[4] Ahcin, P., Sikic, M.. Simulating demand response and energy storage in energy distribution systems. In: 2010 International Conference on Power System Technology. IEEE. ISBN 978-1-4244-5938-4; 2010, p. 1–7. URL: http://ieeexplore.ieee.org/document/5666564/. doi:10.1109/POWERCON.2010.5666564.

[5] Geidl, M., Koeppel, G., Favre-Perrod, P., Klockl, B., Andersson, G., Frohlich, K.. Energy hubs for the future. IEEE Power and Energy Magazine 2007;5(1):24–30. URL: http://ieeexplore.ieee.org/document/4042137/. doi:10.1109/MPAE.2007.264850.

[6] D'hulst, R., Labeeuw, W., Beusen, B., Claessens, S., Deconinck, G., Vanthournout, K.. Demand response flexibility and flexibility potential of residential smart appliances: Experiences from large pilot test in Belgium. Applied Energy 2015;155:79–90. URL: http://dx.doi.org/10.1016/j.apenergy.2015.05.101 http://linkinghub.elsevier.com/retrieve/pii/S0306261915007345. doi:10.1016/j.apenergy.2015.05.101.

[7] Stinner, S., Huchtemann, K., Müller, D.. Quantifying the operational flexibility of building energy systems with thermal energy storages. Applied Energy 2016;181:140–154. URL: http://dx.doi.org/10.1016/j.apenergy.2016.08.055 http://linkinghub.elsevier.com/retrieve/pii/S0306261916311424. doi:10.1016/j.apenergy.2016.08.055.

[8] De Coninck, R., Helsen, L.. Quantification of flexibility in buildings by cost curves Methodology and application. Applied Energy 2016;162:653–665. URL: http://www.sciencedirect.com/science/article/pii/S0306261915013501 http://linkinghub.elsevier.com/retrieve/pii/S0306261915013501. doi:10.1016/j.apenergy.2015.10.114.

[9] Nuytten, T., Claessens, B., Paredis, K., Van Bael, J., Six, D.. Flexibility of a combined heat and power system with thermal energy storage for district heating. Applied Energy 2013;104:583–591. URL: http://linkinghub.elsevier.com/retrieve/pii/S0306261912008227. doi:10.1016/j.apenergy.2012.11.029.

[10] Arteconi, A., Costola, D., Hoes, P., Hensen, J.. Analysis of control strategies for thermally activated building systems under demand side management mechanisms. Energy and Buildings 2014;80:384–393. doi:10.1016/j.enbuild.2014.05.053.

[11] Thomas, Y., Grillet, F., Baetens, R., Alderweireldt, J.. Structural thermal energy storage in heavy weight buildings Analysis and recommendations to provide flexibility to the electricity grid. Tech. Rep.; 3E; Brussels; 2016. URL: https://www.theconcreteinitiative.eu/images/Newsroom/Publications/small_-_3E_StructuralThermalEnergyStorageHeavyWeightBuildings_2016-10-25_Light.pdf.

[12] Zhou, G., Krarti, M., Henze, G.P.. Parametric analysis of active and passive building thermal storage utilization. Journal of Solar Energy Engineering, Transactions of the ASME 2005;127(1):37–46. URL: http://www.engineeringvillage.com/blog/document.url?mid=cpx_765291102e98d762fM689919255120119&database=cpx. doi:10.1115/1.1824110.

[13] Sourbron, M.. Dynamic thermal behaviour of buildings with concrete core activation. Belgium: PhD Thesis, KU Leuven; 2012. ISBN 978-94-6018-572-4. URL: https://lirias.kuleuven.be/handle/123456789/396689.

[14] Sturzenegger, D., Gyalistras, D., Morari, M., Smith, R.S.. Model Predictive Climate Control of a Swiss Office Building: Implementation, Results, and CostBenefit Analysis. IEEE Transactions on Control Systems Technology 2016;24(1):1–12. URL: http://www.opticontrol.ethz.ch/Lit/Stur_13_Proc-Clima2013.pdf http://ieeexplore.ieee.org/document/7087366/. doi:10.1109/TCST.2015.2415411.

[15] Koschenz, M., Lehmann, B.. Thermoaktive Bauteilsysteme TABS. EMPA; 2000. ISBN 3905594196.

[16] Weber, T., Jóhannesson, G.. An optimized RC-network for thermally activated building components. Building and Environment 2005;40(1):1–14. URL: http://linkinghub.elsevier.com/retrieve/pii/S0360132304001544. doi:10.1016/j.buildenv.2004.04.012.

[17] Weber, T., Jóhannesson, G., Koschenz, M., Lehmann, B., Baumgartner, T.. Validation of a FEM-program (frequency-domain) and a simplified RC-model (time-domain) for thermally activated building component systems (TABS) using measurement data. Energy and Buildings 2005;37(7):707–724. URL: http://linkinghub.elsevier.com/retrieve/pii/S0378778804003305. doi:10.1016/j.enbuild.2004.10.005.

[18] Sourbron, M., van der Heijde, B., Battel, B., Vande Ghinste, R., Picard, D., Helsen, L.. Design of a controller model for a concrete core activation floor having air cavities. In: Heiselberg, P.K., editor. CLIMA 2016 - proceedings of the 12th REHVA World Congress: volume 2. Aalborg: Aalborg University, dept. of Civil Engineering; 2016, p. 1–12. URL: https://lirias.kuleuven.be/handle/123456789/536947.

[19] van der Heijde, B., Carrascal Lecumberri, E., Helsen, L.. Experimental Method for the State of Charge Determination of a Thermally Activated Building System (TABS). In: Proceedings of the Greenstock 13th International Conference on Energy Storage. Beijing; 2015,.

[20] Vega Arance, F.J.. Experimental state of charge determination for a floor with concrete core activation. Belgium: Master Thesis, KU Leuven; 2016.

[21] Reynders, G., Diriken, J., Saelens, D.. Bottom-up modeling of the Belgian residential building stock : influence of model complexity. In: 9th International Conference on System Simulation in Buildings (SSB), Liège. Liège (Belgium); 2014, p. 1–19.

[22] Reynders, G., Diriken, J., Saelens, D.. Quality of grey-box models and identified parameters as function of the accuracy of input and observation signals. Energy and Buildings 2014;82:263–274. URL: http://linkinghub.elsevier.com/retrieve/pii/S0378778814005623. doi:10.1016/j.enbuild.2014.07.025.

[23] Cyx, W., Renders, N., Van Holm, M., Verbeke, S.. IEE TABULA - Typology Approach for Building Stock Energy Assessment. Tech. Rep.; VITO; Scientific Report, Mol (Belgium); 2011.

[24] Protopapadaki, C., Reynders, G., Saelens, D.. Bottom-up modelling of the Belgian residential building stock : impact of building stock descriptions. In: 9th International Conference on System Simulation in Buildings (SSB), Liège. Liège (Belgium); 2014, p. 1–21.

[25] Reynders, G.. Quantifying the impact of building design on the potential of structural strorage for active demand response in residential buildings 2015;(September):266. doi:10.13140/RG.2.1.3630.2805.

[26] Patteeuw, D.. Demand response for residential heat pumps in interaction with the electricity generation system. Phd thesis; PhD Thesis, KU Leuven; 2016.

[27] Deurinck, M.. Energy Savings in the Residential Building Sector - An assessment based on on stochastic modelling. Phd; PhD Thesis, KU Leuven; 2015.

[28] Baetens, R., Saelens, D.. Modelling uncertainty in district energy simulations by stochastic residential occupant behaviour. Journal of Building Performance Simulation 2016;9(4):431–447. URL: http://www.tandfonline.com/doi/full/10.1080/19401493.2015.1070203. doi:10.1080/19401493.2015.1070203.

[29] Franck, A.. Karakterisatie van afgiftesystemen - SmartGeotherm. Tech. Rep.; 2013. URL: http://www.smartgeotherm.be/documents/2012/11/karakterisatie-afgiftesystemen.pdf.